



LAWRENCE
LIVERMORE
NATIONAL
LABORATORY

UCRL-JRNL-200853

Testing a Low-Influence Spindle Drive Motor

L. C. Hale, T. A. Wulff, J. C. Sedgewick

**Accepted for publication
March 5, 2004**

Precision Engineering

This document was prepared as an account of work sponsored by an agency of the United States Government. Neither the United States Government nor the University of California nor any of their employees, makes any warranty, express or implied, or assumes any legal liability or responsibility for the accuracy, completeness, or usefulness of any information, apparatus, product, or process disclosed, or represents that its use would not infringe privately owned rights. Reference herein to any specific commercial product, process, or service by trade name, trademark, manufacturer, or otherwise, does not necessarily constitute or imply its endorsement, recommendation, or favoring by the United States Government or the University of California. The views and opinions of authors expressed herein do not necessarily state or reflect those of the United States Government or the University of California, and shall not be used for advertising or product endorsement purposes.

Testing a low-influence spindle drive motor

Layton C. Hale^{a,*}, Timm A. Wulff^a and James C. Sedgewick^b

^a Lawrence Livermore National Laboratory, Livermore, CA 94550, USA

^b Airex Corporation, Dover, NH 03820, USA

Abstract

Precision spindles used for diamond turning and other applications requiring low error motion generally require a drive system that ideally applies a pure torque to the rotating spindle. Frequently a frameless motor, that is, one without its own bearings, is directly coupled to the spindle to make a compact and simple system having high resonant frequencies. Although in addition to delivering drive torque, asymmetries in the motor cause it to generate disturbance loads (forces and moments) which influence the spindle error motion of the directly coupled system. This paper describes the tests and results for a particular frameless, brushless DC motor that was originally developed for military and space applications requiring very low torque ripple. Because the construction of the motor should also lead to very low disturbance loads, it was selected for use on a new diamond turning and grinding machine under developed at Lawrence Livermore National Laboratory. The level of influence for this motor-spindle combination is expected to be of order one nanometer for radial and axial error motion.

Keywords: Slotless, brushless DC motor; Precision spindle; Air bearing; Hydrostatic; Diamond turning; Error motion

1. Introduction

The Lawrence Livermore National Laboratory is developing a new diamond turning and grinding machine for internal use and service to outside customers. With intended capability and capacity to produce visible-light optical surfaces up to 400 mm in diameter, it was given the name Precision Optical Grinder and Lathe (POGAL), though typically many jobs will not be optics. The machine will have four built-in, servo-controlled axes: two B and C spindles mounted respectively on two X and Z slides in a T configuration. Normally we would drive the work spindle with a fairly conventional AC induction motor and variable-frequency drive, and error motion in the motor bearings would be isolated from the spindle with a compliant coupling engineered for low

* Corresponding author. Tel.: 925-422-6823; fax: 925-423-4250

Email address: hale6@llnl.gov.

influence. Because the work spindle must also function as a positioning C axis on this machine, a directly coupled, frameless servomotor provides a more attractive solution if the disturbance loads (principally radial and axial forces) are kept small enough. Unfortunately, motor manufacturers seldom are able to provide radial and axial force data to their customers. In our case, selecting the Airex model RBL7-18521 motor was rather speculative, guided by a basic-level understanding of motor physics and other information to be discussed in Section 2. We purchased the motor then set out to demonstrate through testing whether the radial and axial forces were sufficiently low for direct coupling or whether a compliant coupling and separate motor bearings would be necessary.

The test results of the Airex motor combined with a mathematical model of the POGAL spindle indicate that direct coupling will be quite acceptable. In the radial direction, a constant-amplitude, one-cycle motor force does not cause error motion but rather a static shift of the axis of rotation approximately 6.7 nm [0.26 μin] at the spindle faceplate and 23 nm [0.90 μin] at the end of a 400 mm long workpiece. The residual radial motor force, which is predominantly 12-cycle and proportional to current, could cause nanometer level error motion at the maximum part length during an aggressive finish operation. In the axial direction, a one-cycle motor force appears in the data but it could be an artifact of the test apparatus. If it does exist, the motor rotor could be indexed relative to the spindle to cancel approximately 1 nm of axial error motion inherent in the spindle. The 12-cycle axial force has negligible effect. A future paper is planned to report on the spindle design itself.

1.1. Motor terminology

It may be helpful to define some common terms used to describe various parts and types of motors. Even experts in the field may want to skim this section to be certain that we are using a common vocabulary. We will restrict attention to motors described by the Lorentz force law, but in general the motors may be linear or rotary.

Lorentz force law: $\mathbf{F} = \mathbf{J} \times \mathbf{B}$, where \mathbf{F} is force density, \mathbf{J} is current density and \mathbf{B} is magnetic flux density, all vector quantities [1]. Normally a motor is designed so that \mathbf{J} and \mathbf{B} are perpendicular, thus simplifying and maximizing the cross product. Consider the simple case shown in Figure 1. A length of wire carrying a current ($\mathbf{i} = \mathbf{J} A$) and crossing a magnetic field produces a force equal to the cross product of current times flux density integrated over the length of wire within the field ($\mathbf{f} = \int (\mathbf{i} \times \mathbf{B}) dL$).

Armature: Carries the \mathbf{J} term in the Lorentz force law. Usually it consists of copper wire coils wound in slots in iron laminations, but several other configurations are common.

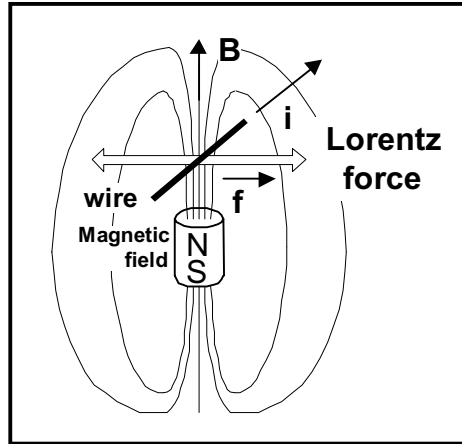


Figure 1 The Lorentz force f is generated perpendicular to the magnetic flux density B and the electric current i flowing through a length of wire.

Field: Carries the B term in the Lorentz force law. Permanent magnets or electromagnets on an iron frame direct the magnetic field to cross the current carrying part of the armature.

Air gap: Refers to the distance that magnetic flux passes through air. Usually it is the physical clearance between the iron laminations of the armature and the field magnets.

Commutation: Refers to the process where current in the armature is synchronized to the field so that those coils immersed in magnetic flux carry current in the proper direction.

Brush DC: Refers to motor commutation using a rotating switch (or commutator) formed usually by carbon brushes rubbing on copper conductors. Usually the brushes and field are stationary and the copper conductors move with the armature.

Brushless DC: Refers to motor commutation using an electronic system rather than a brush-type commutator. Usually the armature is stationary and wound with two or more phases, three being most typical. Brushless AC is another term used synonymously.

Frameless: Indicates that the motor is constructed without bearings. The armature and field are supplied as separate parts, which the customer mounts to a slide or spindle in a prescribed way.

Coreless: Also known as ironless, indicates that the armature has no iron core, contrary to typical motors. The windings and perhaps additional non-conducting fibers are bound in a plastic matrix to form a main structural component of the armature. This structure lies within the air gap.

Slotless: Also known as toothless, indicates that the armature contains iron laminations but lacks the slots that carry the windings in typical motors. The absence of slots presents a continuous ferromagnetic surface to the field magnets and requires the windings to be bound to the iron laminations usually in a plastic matrix. The windings lie within the air gap formed by the iron laminations on one side and the field magnets on the other side.

Torque (or force) constant: Indicates the torque (or force) output of a motor per unit current input. In units of N-m/A (or N/A), the torque (or force) constant is numerically equal to the voltage constant in V-s/r or (V-s/m). For brushless DC motors, the point in the commutation cycle must also be specified, for example, (0.866, -0.866, 0) or (1, -0.5, -0.5) for three phases.

Motor constant: Indicates the torque (or force) output of a motor per square root of heat output under stall conditions. At speed, there are other loss mechanisms giving off additional heat, though typically less significant. The motor constant is computed from the torque (or force) constant divided by the square root of armature resistance. The motor constant decreases somewhat with armature temperature.

1.2. Organization

The body of this paper begins by presenting the considerations leading to the selection of the Airex motor over other options. The bulk of the paper deals with testing the motor, starting with the test apparatus, its calibration and proceeding with the test results. Of particular interest is estimating the motor's influence on spindle error motion. This is accomplished by applying measured radial and axial disturbance forces to a mathematical model of the spindle. Examples include the POGAL spindle and a Professional Instruments 10-inch BLOCK-HEADTM air-bearing spindle.

2. Motor selection

Motors are produced for a wide variety of applications from the very small to the incredibly large, although to our knowledge none are specifically designed for diamond turning spindles. There is active research, however, on motors used for computer disk drives [2], [3]. Apparently motor induced vibration (essentially error motion) is a factor limiting storage density in disk drives. Except for the large difference in size and cost, the two applications are quite similar. The approach used for disc drives has been to examine the relationship of certain motor parameters such as the numbers and proportions of armature slots and field magnets, also known as poles, to performance measures, particularly cogging torque and force imbalance. Choosing slots and poles that interact more frequently per revolution (for example, 9 slots and 8 poles produce 72 undulations) generally reduces the torque with which the motor tends to cog or index. The asymmetry in this combination, however, creates force imbalance. Doubling the number of slots to 18 would restore symmetry and keep the torsional frequency at 72 cycles per revolution.

Choosing a motor based on the numbers of slots and poles seems fairly straightforward but only an expert through detailed analysis could tell if the proportions were also optimized. We consulted Professor Dennis Lieu at the University of California at Berkeley, who co-authored the referenced papers, about the possibility of designing and building a custom motor for our application. When asked about a slotless motor, Professor Lieu agreed that eliminating the slots should lead to less error motion. Without

slots for the magnets to interact with, the motor will have effectively no magnetic cogging or force imbalance other than once per revolution. In addition, manufacturers of slotless motors advertise the torque ripple (i.e., variation in torque constant with angle) to be less than traditional slotted motors. It is possible then that the current-induced radial and axial forces may also be smaller for a slotless design.

Then why use slots? Putting the armature windings in slots allows the air gap to be much smaller leading to more efficient use of available magnetic energy. This is apparent when comparing motor constants between slotted and slotless motor of similar physical size. However, the advent of Neodymium-Iron-Boron magnets has made the discrepancy less of an issue. Thus a slotless motor will be slightly larger and dissipate somewhat more heat than a slotted motor of similar torque capacity. On POGAL, we plan to capture the heat with a temperature-controlled water jacket and size is not a driver.

We narrowed our search to coreless and slotless motors and found several manufacturers who offer standard products at reasonable cost. We down selected to two manufacturers based on these requirements for the POGAL spindle: 1) continuous torque in the 10-15 N-m range, 2) a stationary armature for better heat containment, and 3) frameless construction. Meeting these requirements, Aerotech and Airex offer motors with similar frameless construction, featuring a cylindrical air gap with radial magnetization on the rotor and a slotless stator with three armature phases encapsulated in epoxy. For smaller applications, Maxon, Portescap, ThinGap and Kollmorgen make coreless brush DC and brushless DC motors. Those with built-in motor bearings could have them removed for direct mounting to a spindle.

Having two good options and a need for two motors, we decided to buy the Airex model RBL7-18521 for the work spindle (C axis) and the Aerotech S-180-69-A for the B axis, which is strictly a low-speed positioning axis. Differences in physical size, motor constant and continuous torque (all available from the manufacturers) make each motor somewhat more suitable for its intended use on POGAL. Further confidence came from Airex' experience since the 1980's in developing slotless motors for precision-critical military and space applications [4]. This choice allowed us the opportunity to test both motors, but obtaining similar results, we found no reason to change our plans. Only results for the Airex motor are reported here.

3. Test apparatus

A test stand was developed so that the motor could operate under various conditions while its influence on a spindle was measured, in this case a Professional Instruments 4B BLOCK-HEAD™ air-bearing spindle. As is shown in Figure 2, the motor mounts above the spindle on an aluminum shaft. Above the motor is a one-inch diameter reference ball and two capacitance (or cap) gauges to measure radial and axial motion. The cap gauges mount to the spindle housing through a separate metrology structure. The motor stator

was removed in this particular test to measure the combined error motion of the spindle and ball without influence from the motor. This provides a baseline to compare tests where the motor stator is in place and under power. The stator mounts to a parallel-link flexure stage formed by four rods between the base plate on the right and the motion platform on the left. Displacement of the stator in radial and axial directions correlates to radial and axial force within the motor for frequencies well below mechanical resonance. Not shown are two LVDTs that measure directly against the annular stator. The radial LVDT would be centered on the motor, orthogonal to the spindle axis (see the empty bracket). The axial LVDT would be parallel to but off center from the axis to simplify the mechanical setup. Both the flexure stage and the spindle were calibrated with a force gauge.

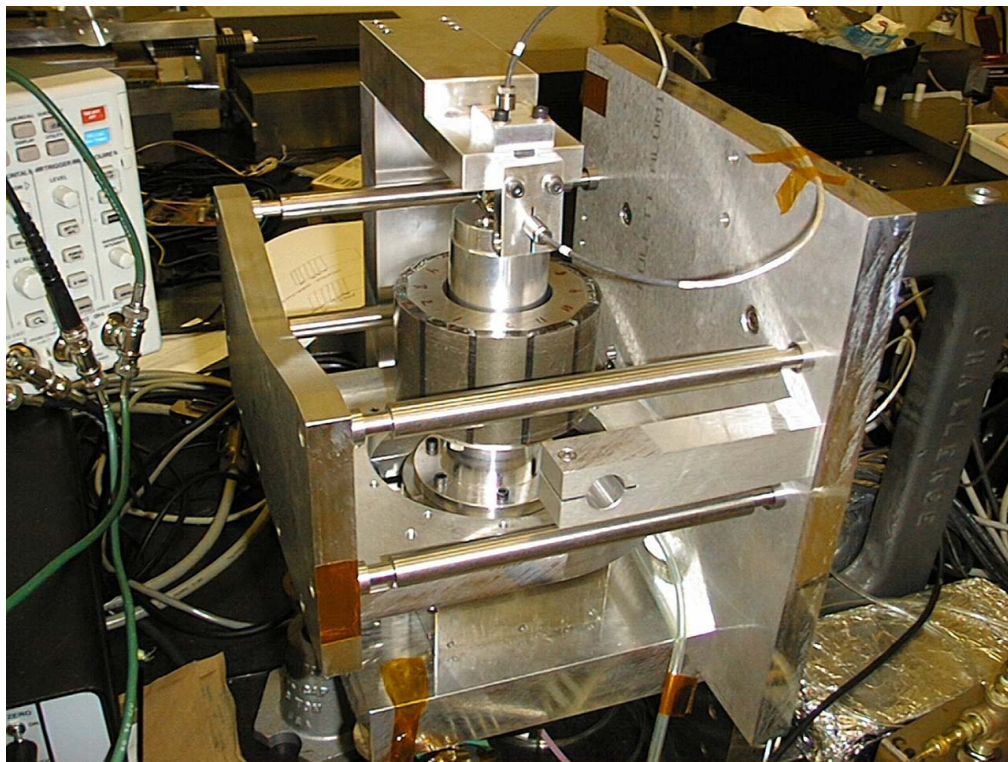


Figure 2 Photograph of the test stand with the motor stator removed.

An Aerotech BA20 three-phase switching amplifier powers the motor under variable current levels set by applying a friction brake to the spindle. The brake was designed to pinch the spindle in a non-influencing way but the level of influence was not determined. The rotation angle of the motor is measured with a Heidenhain ERA180 optical encoder with 9000 sinusoidal cycles per revolution. A Delta Tau PMAC controller commutates the motor, closes the velocity loop and records data from the instruments.

4. Test results

A number of tests were conducted beginning with calibration of the test stand followed by measurements of the magnetic force variation among poles, the back EMF of motor phases, the radial and axial disturbance forces and the radial and axial error motion.

4.1. Calibration for radial and axial force measurements

The flexure stage was calibrated for force by applying up to 75 N through the center of the stator with a force gauge and measuring the displacement with the LVDT. Figure 3 shows straight-line fits to the data collected for axial and radial directions. The slopes are the calibration factors: 0.490 N/ μm for axial and 0.375 N/ μm for radial. The flexure stage by itself has approximately the same stiffness in both directions, but magnetic attraction between the rotor and stator acts as a negative radial stiffness that causes the calibration factors to be different. It is important to consider the consequences of the stator being mounted to a relatively flexible stage compared to a typical mount perhaps 10 to 100 times stiffer. Suppose a radial force of one unit exists between the rotor and the stator on a rigid mount. The flexible mount would allow the stator to move closer to the rotor resulting in a larger force, approximately $0.490/0.375 = 1.31$. Since the stator has been calibrated with the rotor in place, the larger force at the displaced location is equivalent to the calibration test with one unit force applied to the stator. Thus this calibration gives the force equivalent for a rigid mount, as desired.

In a similar manner the spindle was calibrated by applying a force through the center of the rotor with a force gauge and measuring the displacement at the cap gauge. Since the radial force cannot be applied to the rotor with the stator in place, the effect of magnetic attraction is not inherent in this calibration as it is for the flexure stage. A second calibration test is required to account for the larger force that exists when the stator is on a flexible mount compared to a stiff mount. Figure 4 shows the radial displacement measured by the cap gauge for the two calibration tests. In the first test with the stator removed, the radial force is applied to the rotor and the resulting displacement is in the same direction. In the second test, an opposite radial force is applied to the stator causing it to approach the rotor. This movement of the stator causes an attractive force between it and the rotor, which registers on the cap gauge in the same direction as the first test. The appropriate calibration curve comes from adding these two displacements since the disturbance force to be measured is equal and opposite on the rotor and stator, as in the two tests. Figure 4 shows the radial calibration factor to be 3.95 N/ μm .

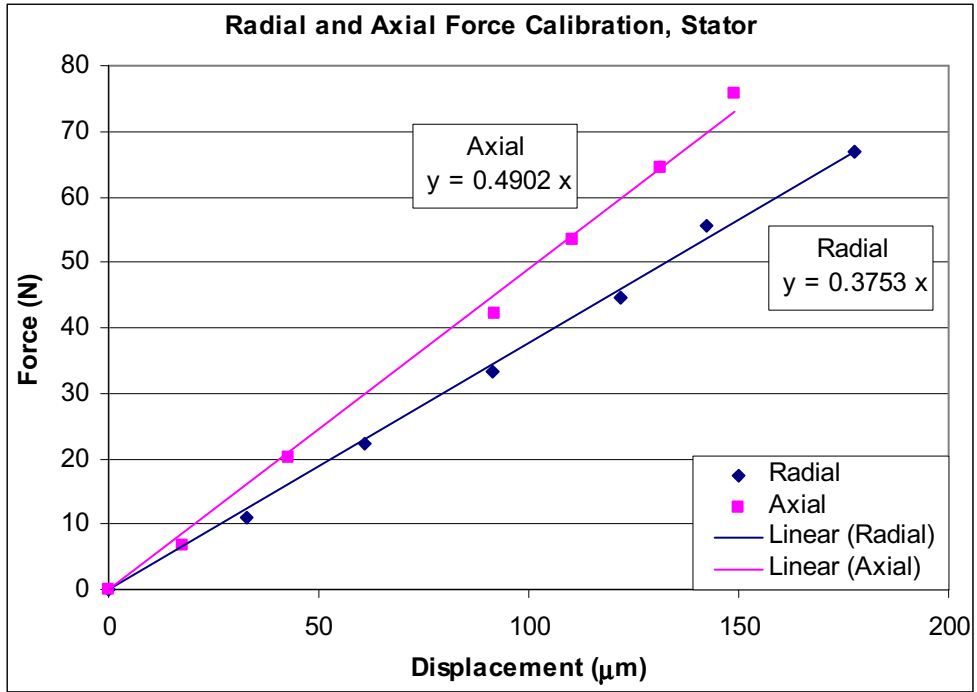


Figure 3 Radial and axial force calibration plots for the flexure stage.

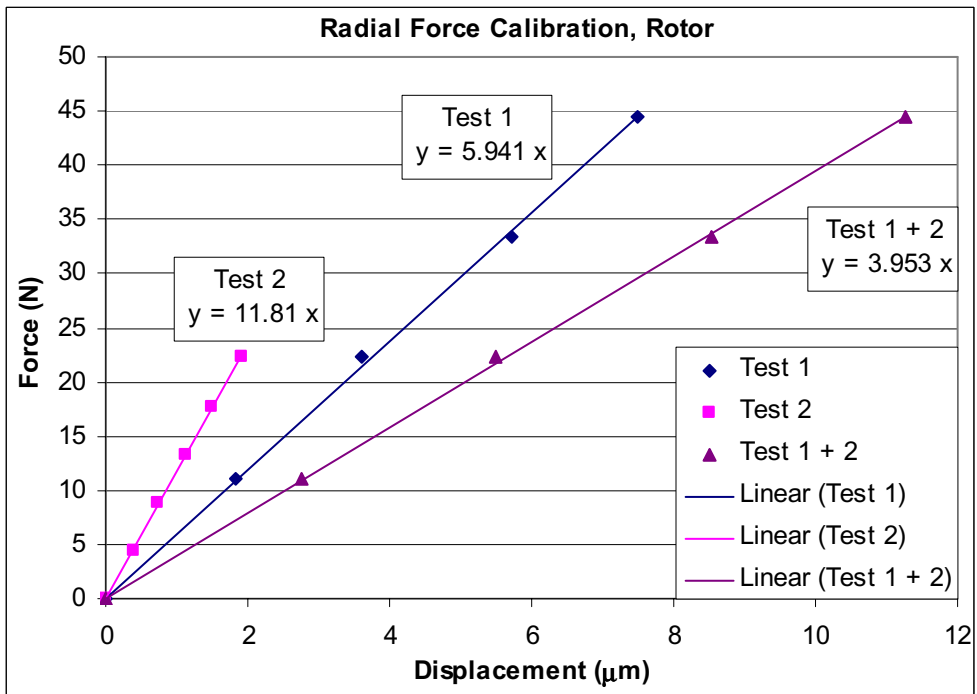


Figure 4 Radial force calibration plot for the spindle rotor.

Figure 5 shows the results of the axial calibration test. A straight-line fit to the data gives the axial calibration factor 170 N/ μm . No correction is required for the flexible

stator mount. The high axial stiffness of the spindle causes the force measurement to be highly quantized and influenced by the inherent error motion in the spindle.

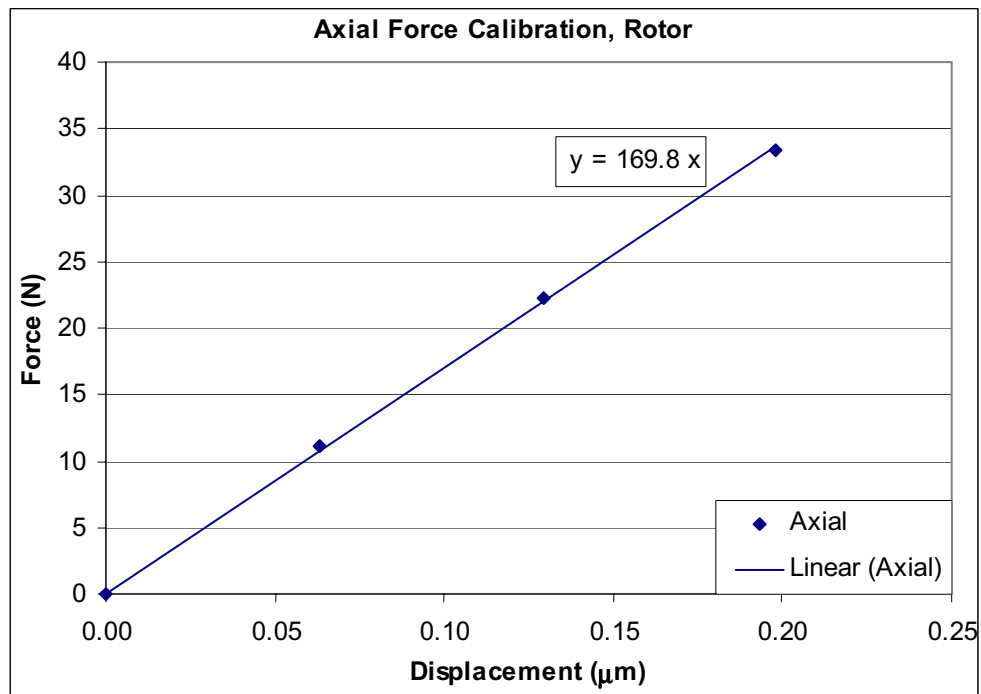


Figure 5 Axial calibration plot for the spindle rotor.

4.2. Magnetic force variations

A steel bar was mounted to the flexure stage in place of the stator to measure the attractive force between it and each of the 12 magnetic poles. The air gap was set to 3 mm as a best guess to an equivalent air gap in the motor, and the bar covered 25 % of the pole area. Table 1 gives the measured forces and the deviations from the average, the greatest being 5.4 %. Figure 6 shows the results as a polar plot. With a magnitude of 1.27 N, the marker near the center indicates the centroid of the measured force. The net radial force on the stator should be at least four times as large (5 N) due to full-area coverage and possibly much greater since the stator iron provides an efficient return path compared to air.

It is also interesting to estimate the magnetic center of the rotor, that is, the axis where the net radial force on the stator would be zero. The ratio of the centroid to the average attractive force, or 1.2 %, multiplied by the 3-mm air gap gives an offset of 0.036 mm between the magnetic center and the spindle axis. This is smaller than the observed runout of the pole surfaces, which suggests that geometric errors may be as significant or more so than variations in magnetic strength. This will be a topic of continued work on the Airex motor.

Magnet No.	Force (N)	Deviation (N)	Deviation (%)
1	104.6	-0.2	-0.2%
2	106.6	1.9	1.8%
3	103.4	-1.4	-1.3%
4	100.6	-4.2	-4.0%
5	101.7	-3.1	-2.9%
6	101.8	-2.9	-2.8%
7	106.2	1.4	1.4%
8	108.3	3.5	3.4%
9	104.3	-0.4	-0.4%
10	105.5	0.8	0.7%
11	110.4	5.7	5.4%
12	103.7	-1.1	-1.0%

Table 1 Attractive force measured between each magnetic pole and a steel bar with a 3-mm air gap and 25 % area coverage. Deviations are from the average of 104.8 N.

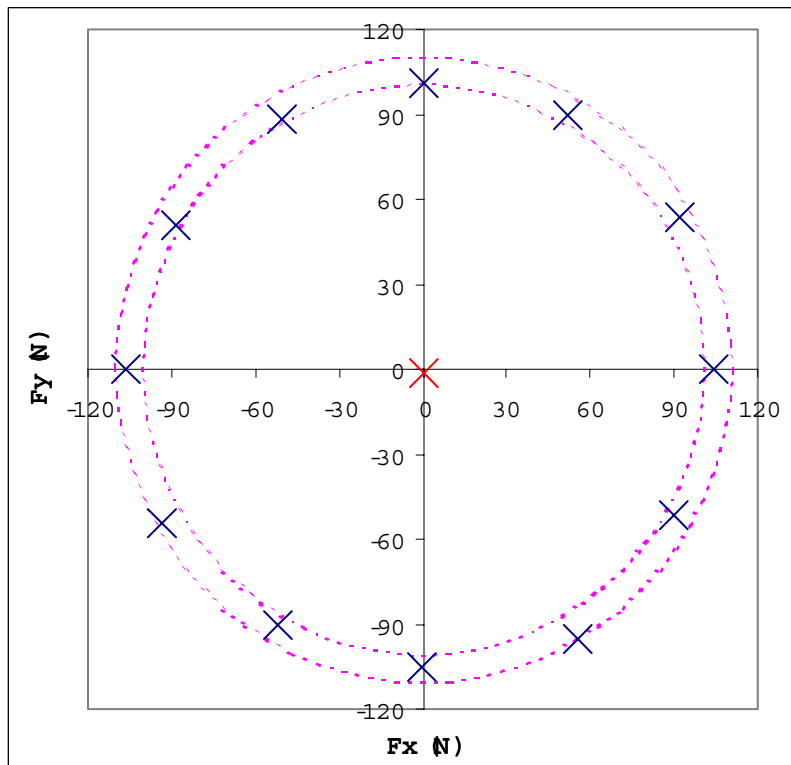


Figure 6 Polar plot of attractive force measurements from Table 1. The centroid is obtained by averaging the x and y components of all 12 radial forces to get $F_x = 0.20$ N and $F_y = -1.26$ N. The polar position is $R = 1.27$ N at -80.7° .

4.3. Back EMF of motor phases

Balance between the three phases of the motor is important to minimize torque ripple and presumably disturbance forces too. The back EMF voltage of each motor phase and the motor angle were sampled at equal time increments while rotating the motor by hand. Dividing the back EMF voltage by the calculated instantaneous velocity normalizes the measurement to a function only of angle. Ideally the function for each phase is sinusoidal with one cycle per pole pair or six cycles per revolution for this motor. Further, all three phases should have equal amplitude and be equally spaced from one another. Figure 7 shows that the three measured functions compare very closely to ideal sinusoids. Applying standard sinusoidal commutation to this motor should give acceptably small variation in the voltage constant. Figure 8 shows the predicted variation, which overall is 2.9 % P-V. The average voltage constant is 1.73 V-s/r for (1, -0.5, -0.5) commutation and 2.00 V-s/r for (0.866, -0.866, 0) commutation. The torque constant is the same value expressed in units of N-m/A.

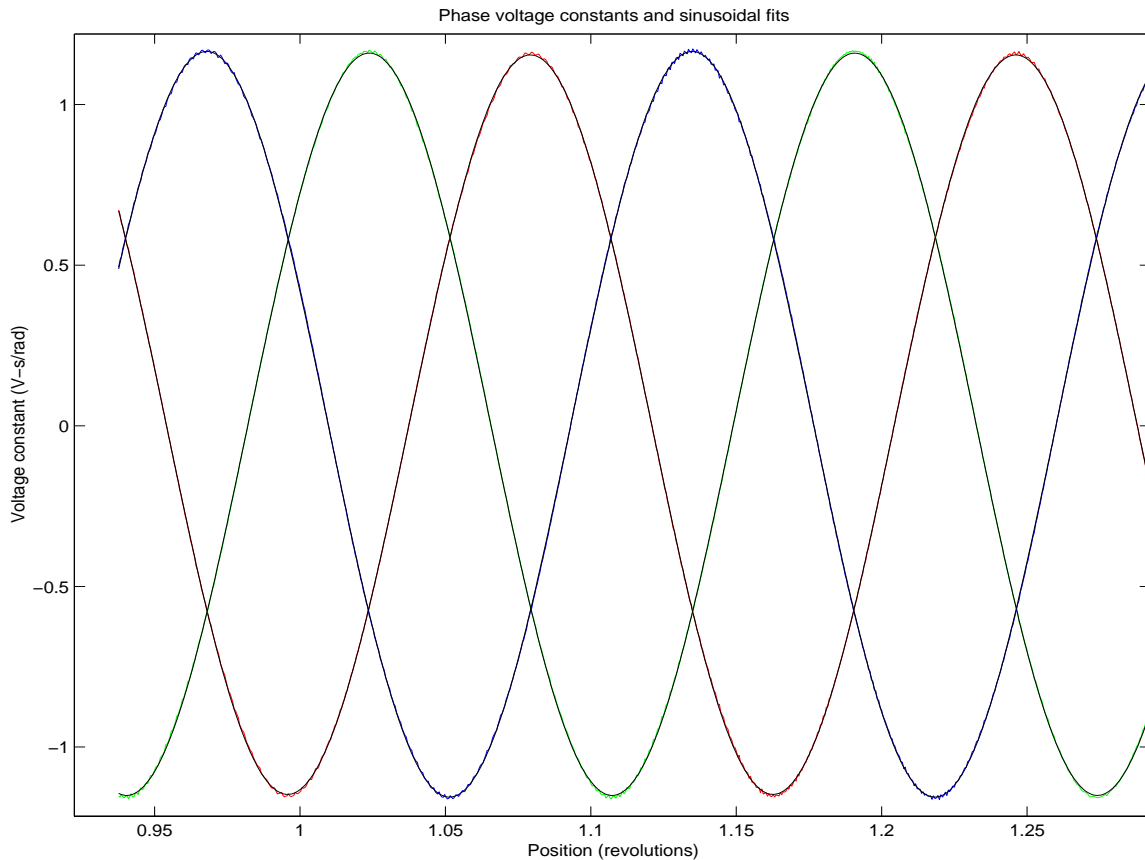


Figure 7 The voltage constant for each phase is very nearly a sinusoidal function of angle. Deviations between the measured (blue, green, red) functions and the ideal sinusoids can be seen near the peaks.

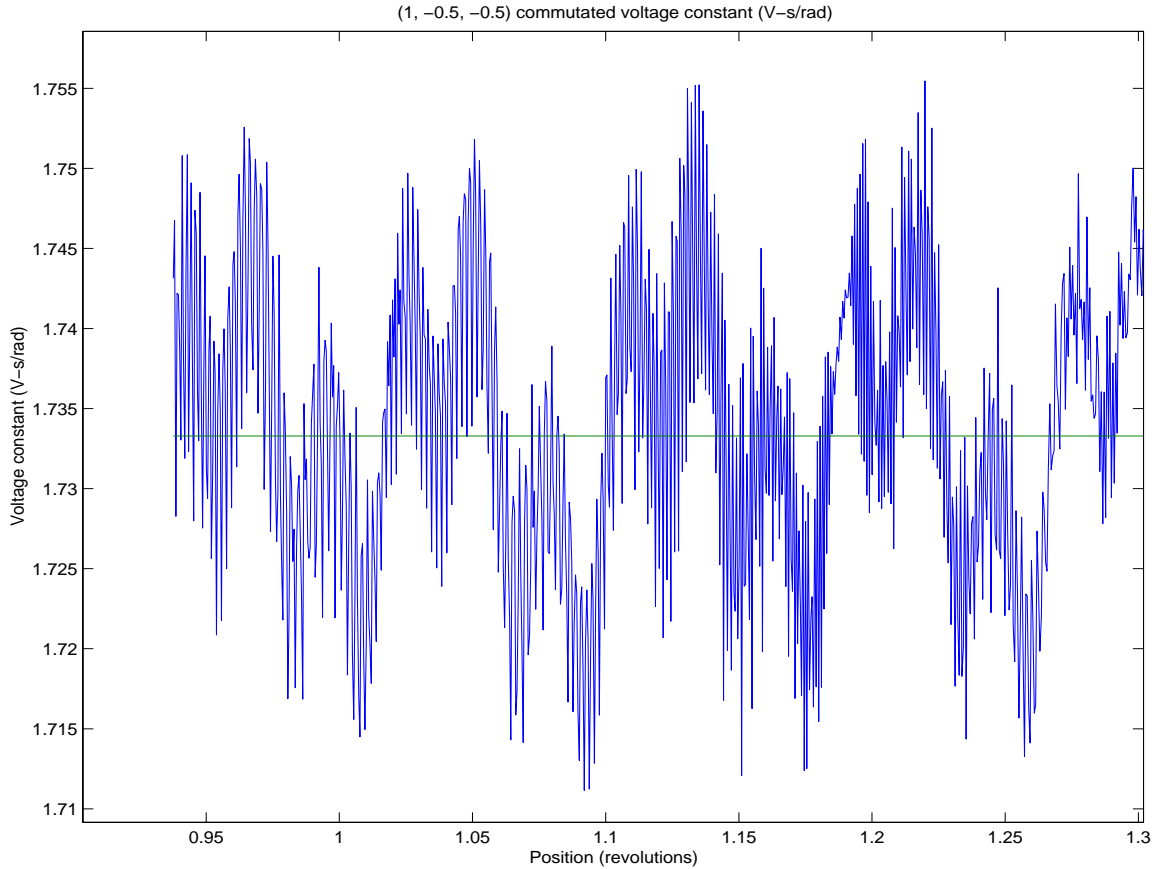


Figure 8 Computed using standard sinusoidal commutation, the voltage constant varies 2.9 % P-V.

4.4. Radial and axial disturbance forces

Radial and axial forces were computed from LVDT and cap gauge measurements using the calibration factors discussed previously. The motor was tested up to 4 A peak, which is 40 % of the continuous current limit of the amplifier and motor. Using the measured torque constant of the motor, the computed torque is 6.9 N-m, not including magnetic hysteresis and inductive losses. The full-speed drag of the spindle bearings is expected to be 2.5 to 3 N-m. A tool load of 20 N at a 200-mm radius—clearly an extreme condition for a finish cut—requires an additional 4 N-m torque from the motor. Thus the 4 A test conservatively represents a worse case finish operation where error motion is of up most concern.

Figure 9 shows the forces for the no-load test of the motor, where the motor drives the spindle without the brake engaged. The radial forces measured independently by the LVDT and cap gauge differ somewhat, 5.6 versus 7.0 N, and are in opposite direction, as they should. The amplitude is relatively large, say 6.2 N, but the period is one revolution, which causes the spindle to rotate true about a slightly shifted axis. The one-cycle radial force is caused by magnetic attraction between the 12 poles on the rotor and the annular laminations of the stator, and the magnitude is close to the predicted

value from the magnetic attraction test. A one-cycle axial force is also present in the data but the magnitude is greater than expected for this motor configuration. It is suspicious that the axial LVDT and cap gauge measurements are not 180° out of phase, as would be the case for a disturbance force between the rotor and stator. There could be some cross coupling in the flexure stage, that is, radial force causing axial motion. If this exists, it would most likely show up 90° out of phase as observed in the data. A later section discusses cross coupling observed in the cap gauge.

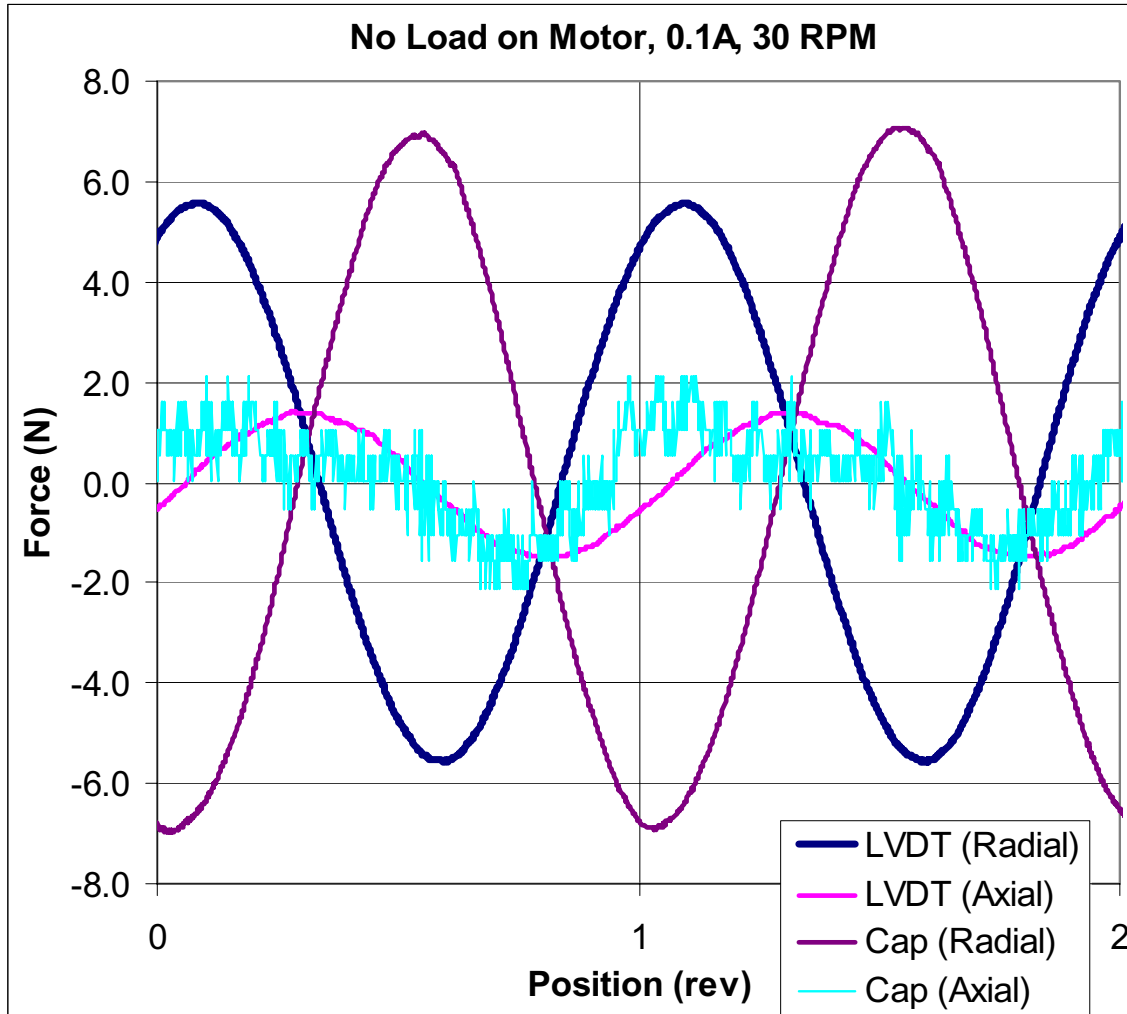


Figure 9 Measured radial and axial forces for minimum current. The two radial measurements are approximately 180 degrees out of phase as expected; however, the two axial measurements are not, indicating the source may be cross coupling rather than axial force.

Figure 10 shows the forces for the 4 A test of the motor, where the motor drives the spindle against the brake. Superimposed on the same one-cycle force is a 12-cycle force ripple that is current dependent. As Figure 11 shows, the one-cycle force is almost constant from 0.1 A to 4.0 A. Figure 12 shows that the amplitude of the 12-cycle force increases somewhat linearly with current in the radial direction and is considerably less significant in the axial direction. Figure 13 compares the radial force occurring for the current extremes, 0.1 A and 4.0 A after having removed the one-cycle force.

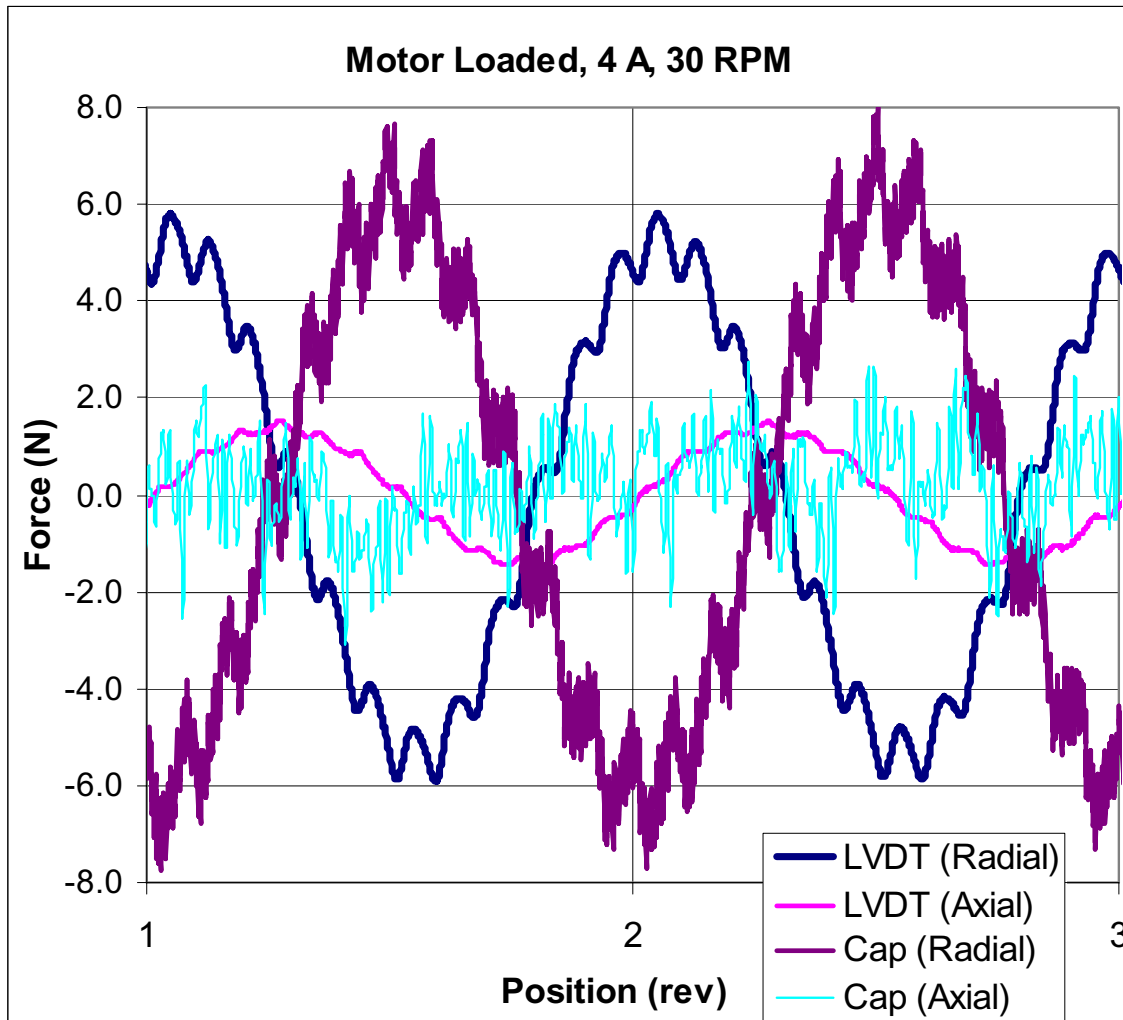


Figure 10 Measured radial and axial forces with the brake set to obtain 4 A peak current. The 12-cycle force ripple results from the applied current.

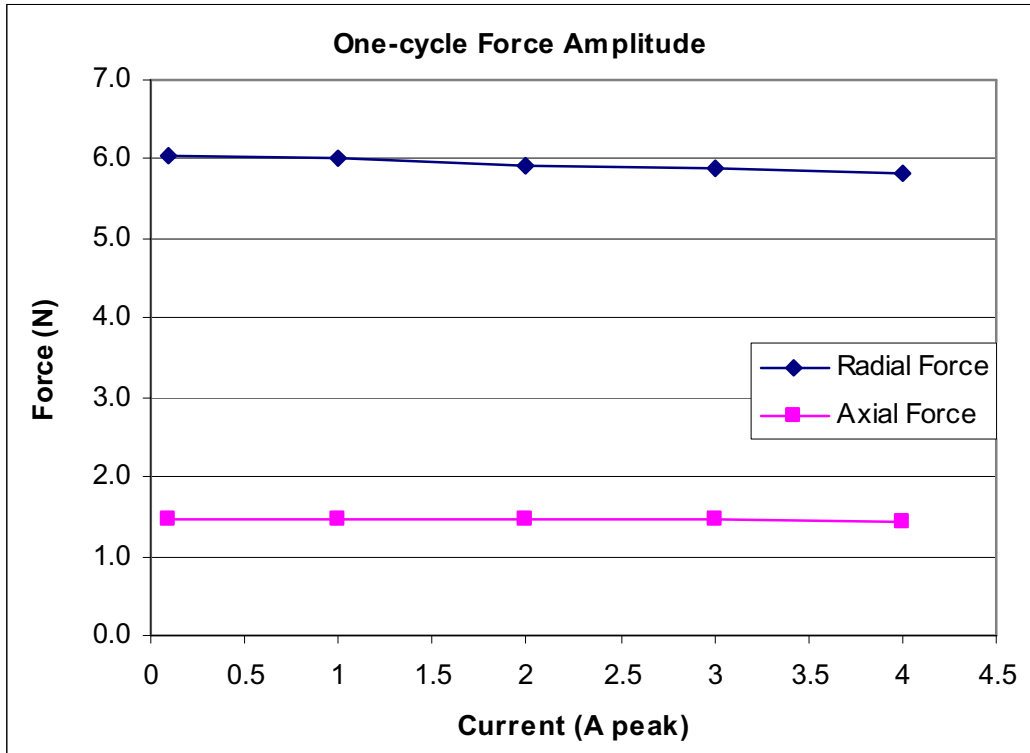


Figure 11 The one-cycle force amplitude is almost constant from 0.1 A to 4.0 A.

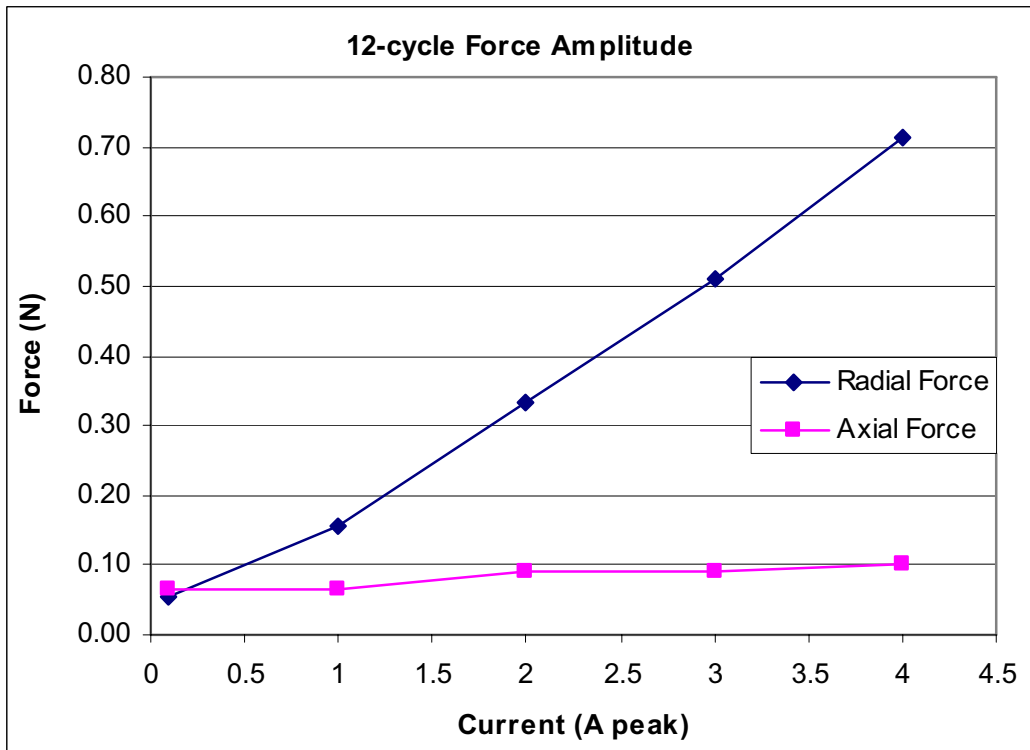


Figure 12 The 12-cycle force amplitude increases somewhat linearly with current in the radial direction.

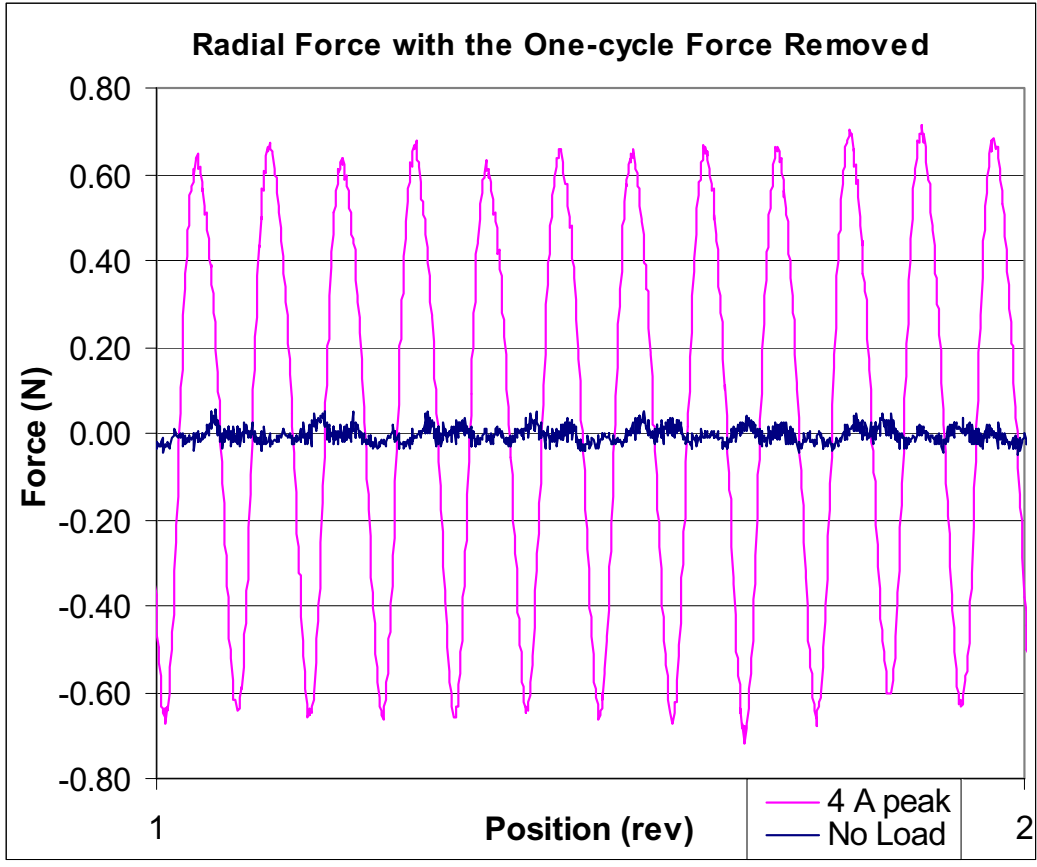


Figure 13 Radial force residual for 0.1 A and 4.0 A with the one-cycle force removed.

4.5. Radial and axial error motion

The cap gauges measure a combination of errors due to the ball, spindle and influence of the motor. Since only the influence of the motor is of particular interest, errors due to the ball and spindle are left combined. A simple way to see the influence of the motor is by comparing the error motion of two tests, one without the stator (zero influence) and a second with the stator in place. For radial error motion, the first harmonic is subtracted out to account for the ball being off center. The ball was only 0.1 μm off center during the baseline test without the stator. In the second test, the radial force between the rotor and stator caused the ball to run approximately 1.8 μm off center. Figure 14 shows the radial error motion for both tests after removing the first harmonic from each data set. Although there is a slight difference (of order 25 nm) apparently caused by the motor, it does not degrade the error motion. In the first test, the rotor was spun by hand and data was collected while coasting. In the second test, the motor was running without the brake applied.

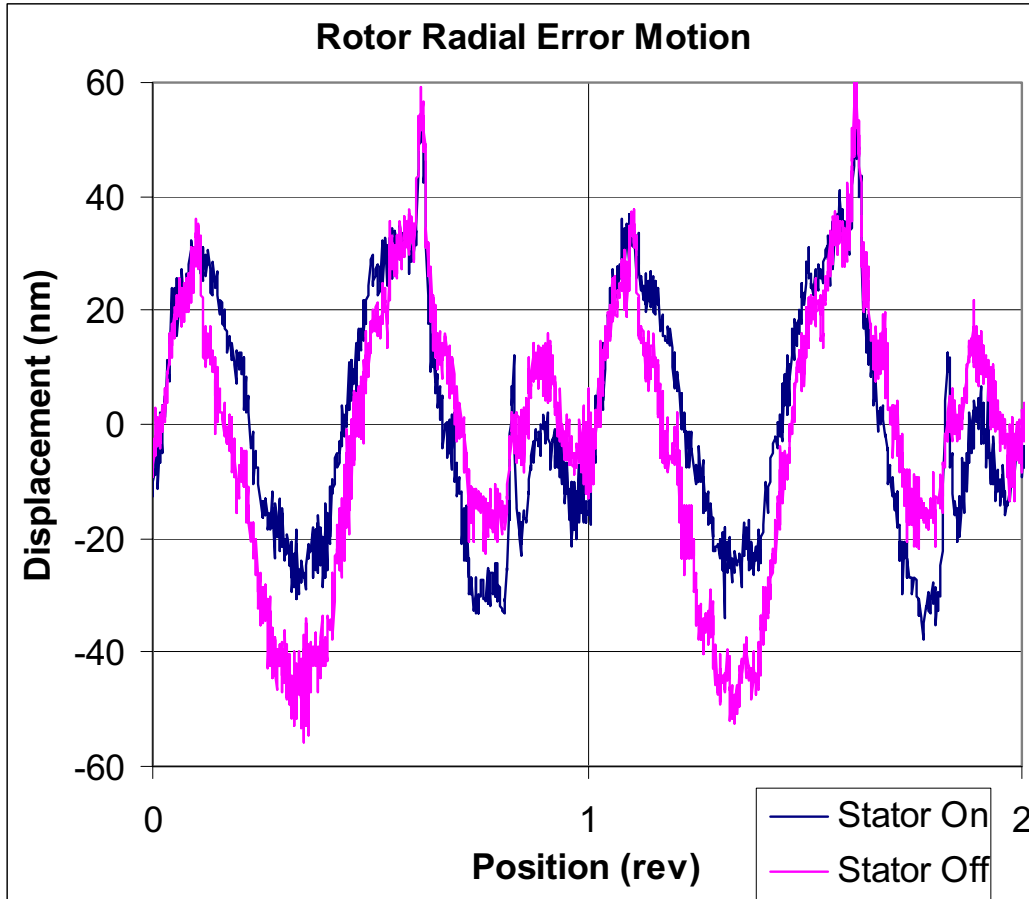


Figure 14 Radial error motion for tests without the stator (zero influence) and with the stator in place.

The same approach is used for axial error motion but there are two differences. First it is inappropriate to subtract the first harmonic. Second, there is some cross coupling between radial motion and axial measurement. Another baseline test was made without the stator where the ball was purposely moved off center to closely duplicate the cross coupling that occurs with the stator in place. Figure 15 shows the axial error motion for the new baseline and the test with the stator in place. The pronounced one-cycle error comes largely from cross coupling. It would be better to center the ball for both test, but these results show that the influence of the motor is minor and actually helpful in this case. Thus, it should be possible to index the rotor so that any one-cycle force tends to cancel any one-cycle error inherent in the spindle.

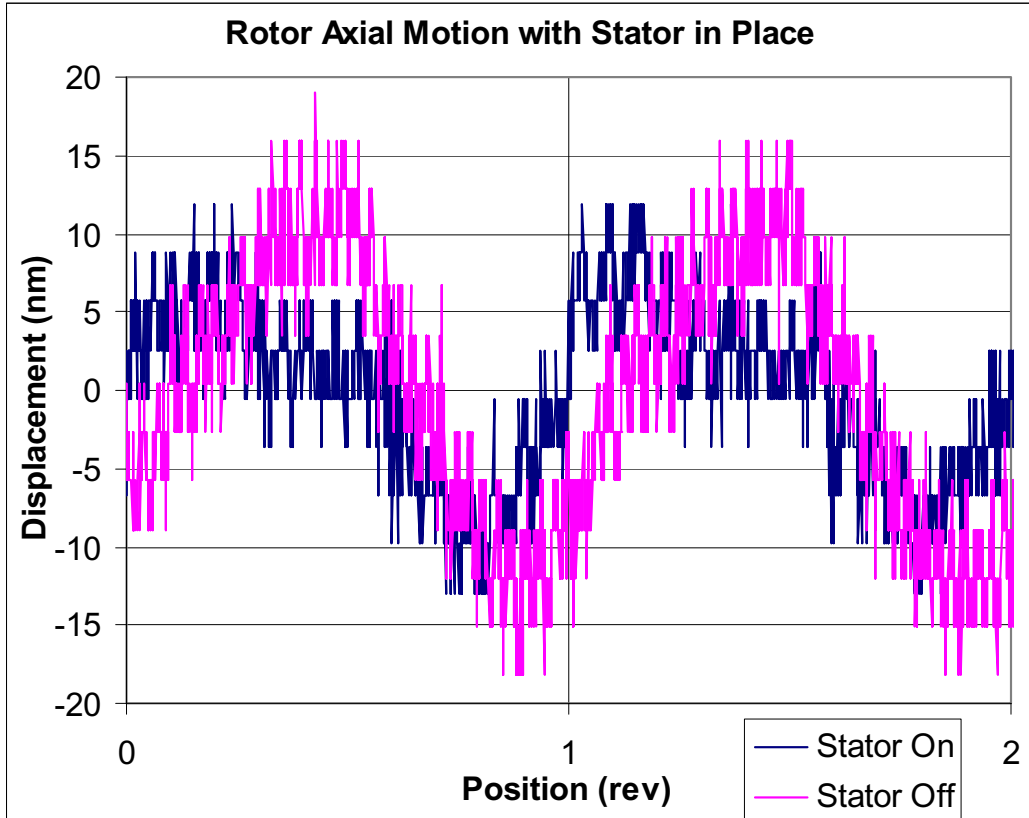


Figure 15 Axial error motion for tests without the stator (zero influence) and with the stator in place. The balls are similarly off center in both tests to have similar amounts of cross coupling from radial motion.

5. Error motion estimate for the POGAL hydrostatic spindle

The radial and axial forces measured for the Airex motor will now be applied to the mathematical model of the POGAL spindle to estimate the effect on error motion. The spindle configuration is fairly conventional with front and rear journal bearings, an annular thrust bearing, and the motor overhanging in the rear. The model includes the compliance of the hydrostatic bearings and the bending and shear compliance of the spindle rotor. The spindle is most compliant under static loading and stiffens somewhat with increasing frequency due to squeeze-film damping in the bearings. The POGAL control system will have the ability to sense and reduce any significant error motion for frequencies sufficiently below the position-loop bandwidth.

5.1. Radial error motion estimate

A radial force at the motor causes radial displacement of the front and rear journal bearings in opposite directions, thus causing the spindle to rock about a nodal point in between. To a lesser extent the spindle rotor bends but this effect actually reduces radial displacement at the workpiece. This behavior is evident in Equation 1, where the parameters used in the model appear in Table 2. As one would expect, it is desirable to minimize the overhang of the motor and workpiece relative to the span between bearings

(all lengths are with respect to bearing centers). The two bearings share more or less equally in the total displacement depending on the relative length of the workpiece, with the front being more significant for short parts and the rear being more significant for long parts.

$$\delta_r(\omega) := f_{m,r} \left[\frac{a \cdot b \cdot L}{6 \cdot E \cdot I} - \frac{2 \cdot (1 + \nu) \cdot a \cdot b}{E \cdot A_s \cdot L} - \frac{b \cdot (a + L)}{k_a(\omega) \cdot L^2} - \frac{a \cdot (b + L)}{k_b(\omega) \cdot L^2} \right] \quad (1)$$

<i>Symbol</i>	<i>Description</i>	<i>Value</i>	<i>Unit</i>
k_a	Stiffness of front journal bearing	$1330 + i \omega 4.62$	N/ μ m
k_b	Stiffness of rear journal bearing	$533 + i \omega 2.77$	N/ μ m
a	Workpiece lever arm (three cases)	114, 318, 521	mm
b	Motor lever arm	171	mm
L	Span between front and rear bearings	381	mm
D	Outer diameter of spindle rotor	152.4	mm
d	Inner diameter of spindle rotor	41.3	mm
I	Area moment of inertia, I(D,d)	2.634E+7	mm ⁴
A_s	Effective shear area, $A_s(D,d)$	1.448E+4	mm ²
E	Elastic modulus	207	GPa
ν	Poisson ratio	0.3	

Table 2 Parameters used in the spindle model for estimating radial error motion. The bearing stiffness is a complex function of frequency to include squeeze-film damping. The three cases of workpiece lever arm correspond to spindle faceplate, center of work volume and maximum work volume.

Although the 6.2 N one-cycle radial force does not cause error motion, it is interesting to compute the shift it causes to the axis of rotation. Applying this to the model causes shifts of -6.7, -15 and -23 nm [-0.26, -0.58, -0.90 μ m] at three places in the work volume: the spindle faceplate, the center and the maximum length workpiece. These values would diminish somewhat with increasing spindle speed (15 % from zero to maximum speed). This is a negligible change in shift versus speed under normal machining circumstances.

The 12-cycle radial force does cause error motion and the value measured for the 4 A test, 0.7 N, is applied to the spindle model to obtain the estimate. Figure 16 shows how the error motion varies with frequency and location in the work volume. Even the largest value, -2.6 nm, is tolerable compared to an optimistic goal for the error motion inherent in the spindle. Consider operating the spindle at 500 rpm where the 12-cycle force has a frequency of 100 Hz. The influence of the motor falls to approximately -1 nm at the maximum length workpiece.

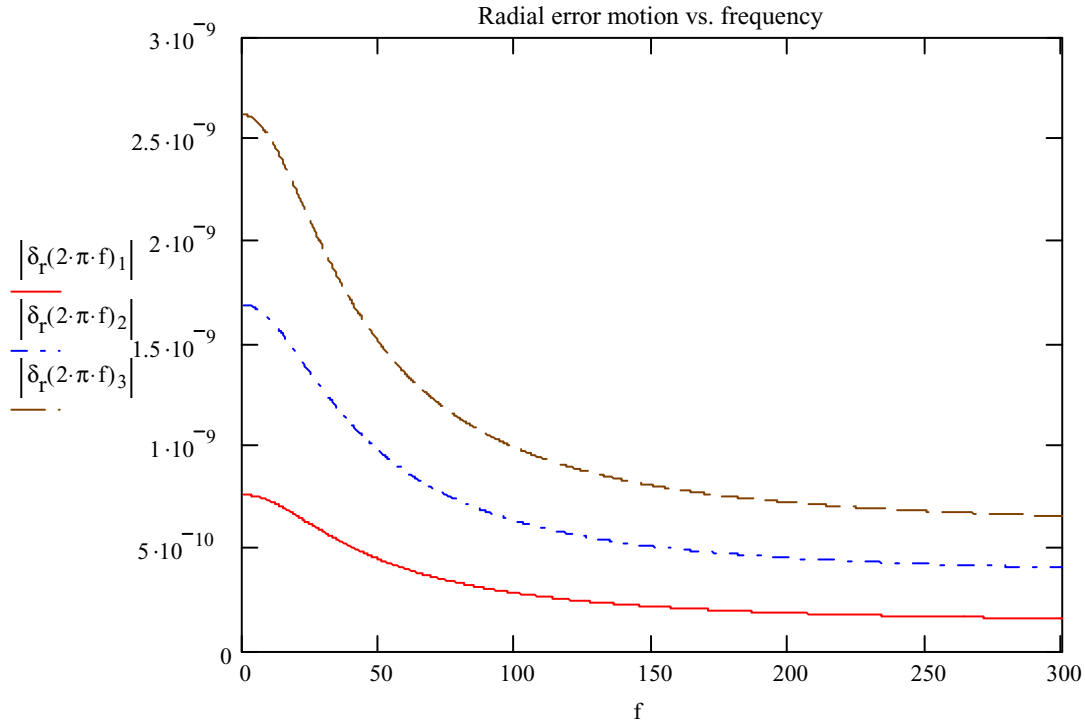


Figure 16 A motor current of 4 A causes error motion (in meters) that varies with frequency (in Hz) and location in the work volume.

5.2. Axial error motion estimate

The axial force of the motor acts directly against the thrust bearing so the compliance of the spindle rotor is not a factor. The axial stiffness predicted for the thrust bearing is $(1610 + i \omega 1.56)$ N/ μ m. The 1.5 N one-cycle axial force, much of which is likely an artifact of the test apparatus, would produce 0.93 nm [0.037 μ in] amplitude of axial motion, diminishing somewhat with frequency. Assuming this is real and can be reliably determined, the rotor could be indexed to reduce slightly the one-cycle error motion inherent in the spindle. The 0.1 N 12-cycle axial force measured for the 4 A test would not be detectable at 0.062 nm [0.0024 μ in]. Clearly there is no issue with the Airex motor influencing axial error motion of the POGAL spindle.

6. Error motion estimate for a 10-inch BLOCK-HEAD™ air-bearing spindle

The radial and axial forces measured for the Airex motor will now be applied to a 10-inch BLOCK-HEAD™ air-bearing spindle using specifications published by Professional Instruments to estimate the effect on error motion [5]. Only quasi-static operation will be considered. The spindle configuration is quite different from that planned for POGAL. It has one journal bearing and a large annular thrust bearing for both axial and moment stiffness. The motor overhangs in the rear and the workpiece overhangs in the front.

6.1. Radial error motion estimate

A radial force at the motor causes radial displacement of the journal bearing and tilt of the thrust bearing as described in Equation 2, where the spindle rotor is assumed to be rigid since any bending would actually reduce displacement at the workpiece. We will use the same lever arms for the motor and workpiece as was used previously. Table 3 lists the parameters used in the model.

$$\delta_r := f_{m,r} \left(\frac{1}{k_r} - \frac{a \cdot b}{k_m} \right) \quad (2)$$

<i>Symbol</i>	<i>Description</i>	<i>Value</i>	<i>Unit</i>
k_r	Radial stiffness of journal bearing	350	N/ μ m
k_m	Tilt stiffness of thrust bearing	11.3	N-m/ μ r
a	Workpiece lever arm (three cases)	114, 318, 521	mm
b	Motor lever arm	171	mm

Table 3 Parameters used in the spindle model for estimating radial error motion. The three cases of workpiece lever arm correspond to spindle faceplate, center of work volume and maximum work volume.

The 6.2 N one-cycle radial force causes the axis of rotation to shift by 7.0, -12 and -31 nm [0.27, -0.48, -1.2 μ in] at the three workpiece lever arms. The location of the nodal point, where $\delta_r = 0$, is $a = 188$ mm, which is within the work volume. The 0.7 N 12-cycle radial force for the 4 A test causes error motion in the amounts of 0.79, -1.4 and -3.5 nm [0.031, -0.054, -0.14 μ in] at the three workpiece lever arms.

6.2. Axial error motion estimate

The axial stiffness specified for the thrust bearing is 1750 N/ μ m. The 1.5 N one-cycle axial force, if it exists, would produce 0.86 nm [0.034 μ in] amplitude of axial motion, which could be indexed to reduce slightly the one-cycle error motion inherent in the spindle. The 0.1 N 12-cycle axial force measured for the 4 A test would not be detectable at 0.057 nm [0.0023 μ in]. Clearly there is no issue with the Airex motor influencing axial error motion of the BLOCK-HEADTM spindle.

7. Summary

The test results for the Airex motor combined with a mathematical model of the POGAL spindle indicated that the additional error motion caused by the motor will be tolerable and probably quite difficult to even observe in the midst of other error sources. The slotless design of the motor integrates the pull of 12 slightly different pole magnets to a constant rotating radial force on the spindle causing only a shift of the axis of rotation, not error motion. If there is a small one-cycle axial force, the rotor can be indexed to partially cancel the axial error motion inherent in the spindle. Non symmetries in the magnets and windings cause 12-cycle radial and axial forces proportional to current,

though probably much smaller and smoother than in a motor with slots. The effect on the spindle is tolerable in the radial direction and negligible in the axial direction. Conservatism has been built into these estimates particularly in the level of current, and the bearing design can be made more robust now with a better understanding of the key parameters involved.

Acknowledgments

This work was performed under the auspices of the U.S. Department of Energy by the University of California, Lawrence Livermore National Laboratory under contract No. W-7405-Eng-48.

References

- [1] Fitzgerald AE, Kingsley C, Umans, SD. Electric machinery, 5th ed. McGraw-Hill, 1990. pp 96-97.
- [2] Kim U, Lieu DK. Analytical Techniques for Magnetically Induced Vibrations in Brushless Permanent-Magnet Motors. J. Info. Storage Proc. Syst., 1999;1;211-216.
- [3] Wang JP, Chuang TY, Lieu DK. Design Techniques for Spindle Motors in Data-Storage Devices. J. Info. Storage Proc. Syst., 1999;1;105-114.
- [4] Airex Corporation website: <http://www.airex.com/>
- [5] Professional Instruments website: <http://www.airbearings.com/>